Understanding the Anchoring Effect of Two-Dimensional Layered Materials for Lithium−Sulfur Batteries

Qianfan Zhang,*,†,‡ Yapeng Wang,† Zhi Wei Seh,‡ Zhongheng Fu,† Ruifeng Zhang,† and Yi Cui*,‡,§

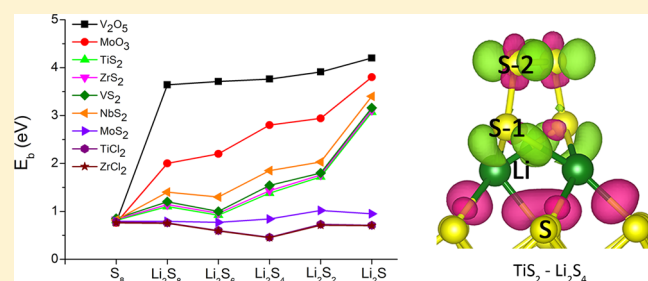†School of Materials Science and Engineering, Beihang University, Beijing, 100191, P. R. China

‡Department of Materials Science and Engineering, Stanford University, Stanford, California 94305, United States

§Stanford Institute for Materials and Energy Science, SLAC National Accelerator Laboratory, Menlo Park, California 94025, United States

S Supporting Information

ABSTRACT: Although the rechargeable lithium−sulfur battery system has attracted significant attention due to its high theoretical specific energy, its implementation has been impeded by multiple challenges, especially the dissolution of intermediate lithium polysulfide (Li_2S_n) species into the electrolyte. Introducing anchoring materials, which can induce strong binding interaction with Li_2S_n species, has been demonstrated as an effective way to overcome this problem and achieve long-term cycling stability and high-rate perform-ance. The interaction between Li_2S_n species and anchoring materials should be studied at the atomic level in order to understand the mechanism behind the anchoring effect and to identify ideal anchoring materials to further improve the performance of Li−S batteries. Using first-principles approach with van der Waals interaction included, we systematically investigate the adsorption of Li_2S_n species on various two-dimensional layered materials (oxides, sulfides, and chlorides) and study the detailed interaction and electronic structure, including binding strength, configuration distortion, and charge transfer. We gain insight into how van der Waals interaction and chemical binding contribute to the adsorption of Li_2S_n species for anchoring materials with strong, medium, and weak interactions. We understand why the anchoring materials can avoid the detachment of Li_2S as in carbon substrate, and we discover that too strong binding strength can cause decomposition of Li_2S_n species.

KEYWORDS: lithium−sulfur battery, anchoring material, two-dimensional layered materials, first-principles simulation, Li_2S_n species

Rechargeable lithium-ion batteries are widely used in many applications owing to their high energy density, long lifetime, and lightweight design. However, the current cathodes in consumer electronics market possess a limited theoretical specific capacity of ∼300 mAh/g, which cannot fulfill the increasing energy demands of modern society, especially the urgent needs of energy storage for vehicle electrification and grid scale applications.[1−5] Sulfur cathode has a specific capacity of 1673 mAh/g, which gives lithium−sulfur batteries a specific energy of 2600 Wh/kg, more than five times higher than the conventional lithium-ion batteries based on metal oxide cathodes and graphite anodes. Furthermore, the low cost and low toxicity of sulfur makes it attractive for commercial applications.[6,7] Despite all of these advantages, successful implementation of lithium−sulfur batteries has been hindered by a series of obstacles, including poor cycle life, low Coulombic efficiency, and low active material utilization,[7−18] which are caused by three main reasons: (i) dissolution of lithium polysulfide (Li_2S_n) species into the electrolyte, (ii) low ionic/electronic conductivity of both sulfur and lithium sulfide, and (iii) large volumetric expansion of sulfur (∼80%) upon lithiation.

Nanostructure designs of cathodes have been demonstrated as the effective way to overcome the problems listed above. Extensive research has confirmed that micro/nanostructured carbon-based materials[19−25] can lead to improvement in the specific capacity and cycling performance of lithium−sulfur batteries. However, our earlier study showed that these nonpolar carbon-based materials possess weak interaction with polar Li_2S_n species, which lead to detachment of Li_2S from the carbon surface and hence, poor cycling performance.[26] This proves that carbon-based materials alone cannot serve as an ideal matrix, and further modification on the interface between carbon and sulfur is needed to avoid the sulfur cathode decay. We pointed out that having polar function groups is important to increase the interaction between Li_2S_n species and electrode.[26] Following that, extensive work has been done on introducing oxygen functional groups on carbon that can better anchor Li_2S_n species, or replacing carbon with other polar materials. Now, introducing nanoscale anchoring material is
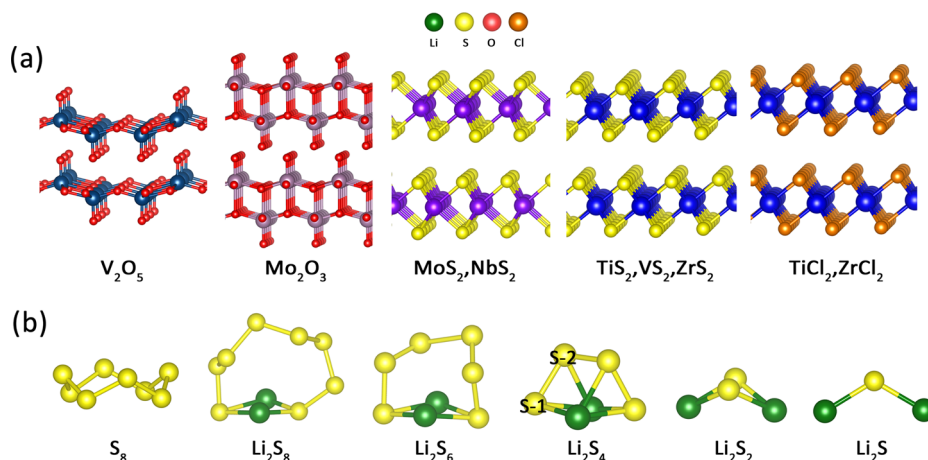
Figure 1. (a) Illustration for atomic structure of layered materials that are used as anchoring materials. (b) Molecule configurations for Li−S composites at various lithiation stages, from unlithated S_8 to Li_2S_2. Here, blue, yellow, and green balls symbolize oxygen, sulfur, and lithium atoms, respectively. Balls with other colors symbolize various metal atoms.

viewed as one of the most important methods to confine the Li_2S_n species and avoid their dissolution.[26−36] To date, various types of polar nano-AMs including polymers (polyaniline, polypyrrole, PEDOT),[26−28] metal oxides (SiO_2, TiO_2, Al_2O_3),[29−35] and most recently, transition metal disulfides (TiS_2, ZrS_2, VS_2)[36] have been demonstrated to enhance the battery performance.

Due to lack of microscopic insight into the interaction features between AM and Li_2S_n species, the choice of AM to use is largely empirical in nature. A number of modeling simulations have been carried out on anchoring effect of AMs using simplified Li−S molecule models,[26−28,36] which is very helpful for selecting suitable AM and estimate the binding strength. However, it is still far from a clear clarification of the interaction mechanism. First, people usually select individual lithiation spot for modeling, especially the fully lithiated species like Li_2S. Such simulation can not gain the trend of anchoring effect and the evolution of adsorption situation during overall lithiation process, especially the under-/middle-lithiated molecule-formimg stages with large n. Therefore, the entire-lithiation-process computation is very important. Second, AMs are mainly evaluated by the induced binding strength, and it is commonly believed that the stronger binding the better. A comprehensive electronic structure calculation and analysis needs to be carried out for a better understanding of Li_2S_n−AM system, including the detailed physical or chemical interaction, charge transfer, adsorption configuration, and structural stability, in order for a more rational design of cathode. Third, the choice of AMs that have been tried is limited, and the comparative study including various AMs need to be done in order to investigate different anchoring trend induced by different AMs, especially the distinction between carbon and AMs like oxides or sulfides. Therefore, a systematic simulation study, covering AMs with different binding strengths and Li_2S_n species at different lithiation stages (n = 1−8), is required. In this paper, we present a systematic investigation on the anchoring effect of layered materials with reference to carbon and clarify the mechanism of their anchoring effect and interaction electronic structure with Li_2S_n species. On the basis of the insight gained, we suggest possible ideal anchoring materials that can be used to further improve the performance in Li−S batteries.

■ METHOD

The computations were performed using the Vienna ab initio simulation package (VASP) in the framework of density functional theory (DFT).[37,38] The projector augmented wave (PAW) pseudopotential was adopted and the GGA exchange-correlation function was described by Perdew−Burke−Ernzerhof (PBE).[39,40] Particularly, we used the vdW-DF2 functional to include the physical van der Waals (vdW) interaction in the simulation,[41,42] which was not included in previous studies,[36] but we will show it is very important in the following text. All the calculations were carried out using this scheme unless otherwise specified. The AMs we selected are materials with layered structure for two main reasons. First, layered materials have been widely used as electrode materials,[43] and most recently, layered sulfides have been demonstrated as excellent AMs in Li−S batteries as well.[36] Second, the layered materials can avoid introducing dangling bond or reconstruction on the surface, which may lead to unreliable binding strength, and can be served as ideal interaction models. Here, we study various layered oxides (V_2O_5, MoO_3), sulfides (TiS_2, VS_2, ZrS_2, NbS_2, MoS_2), and chlorides ($TiCl_2$ and $ZrCl_2$) shown in Figure 1a, which can cover the broad range of binding strength with Li_2S_n species, as we will show. To simulate AM, few-layer (2−3 layers) supercell structures, with two-dimensional periodicity in $x−y$ plane, are used. For most of the simulations, we study the full set of S-related species including S_8, Li_2S_8, Li_2S_6, Li_2S_4, Li_2S_2 and Li_2S, which represent the critical lithiation stages demonstrated by experiments.[44] Figure 1b shows the stable configurations for these molecules according to our simulations. All the Li_2S_n species (n = 1−8) are in a three-dimensional cluster shape instead of chains with Li atom on the terminals, which is usually supposed to be.[44] Other simulation works also support this point.[45] The binding energy, E_b, is computed to measure the binding strength between these Li_2S_n species and the AM. It is defined as the energy difference between the Li_2S_n−AM adsorbed system (E_{Li_2Sn+AM}) and the summation of pure Li_2S_n (E_{Li_2Sn}) and pure AM (E_{AM}) and can be expressed as $E_b = E_{Li_2Sn} + E_{AM} − E_{Li_2Sn+AM}$. With this definition, a positive binding energy indicates that the binding interaction is favored. All the E_b magnitudes and atomic configurations showed below are those of the most stable adsorption cases.

■ RESULTS AND DISCUSSIONS

First, we calculate the adsorption of S_8 and Li_2S_n species ($n = 1-8$) on graphene to investigate why these species cannot adhere strongly on the carbon-based substrate. Each of the above-mentioned species shown in Figure 1b is placed on top of crystalline graphene (c-G) or amorphous graphene (a-G) layer (see Section 2 of Supporting Information for details), respectively, and the lithiation evolutions of binding energy are plotted as black and red solid curves in Figure 2a. For S_8
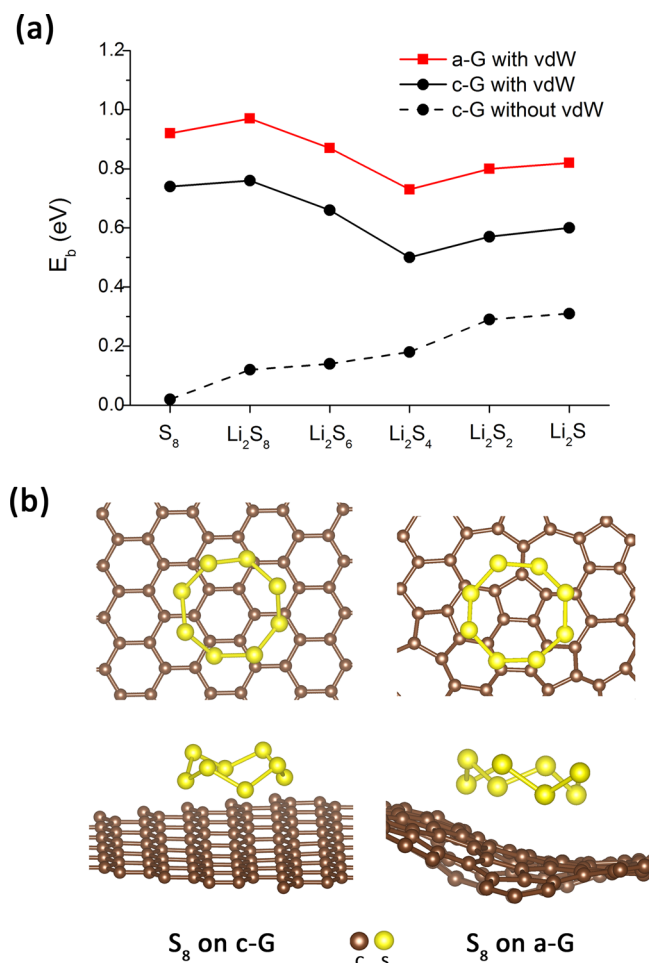

Figure 2. (a) Adsorption binding energies for Li–S composites on graphene. Solid black and red curves represent crystalline graphene (c-G) and amorphous graphene (a-G), respectively, using the simulation method with vdW functional. Dashed black curve represents crystalline graphene case without considering vdW interaction. (b) Atomic configurations for S_8 cluster's adsorption on c-G (left side) and a-G (right side), both top view (up) and side view (down) are shown.

molecular cluster, the initial unlithiated stage, the stable adsorption configurations on c-G and a-G substrates are shown as Figure 2b, and the binding energies are 0.74 and 0.92 eV, respectively. The binding energy for Li_2S_8 is slightly larger than S_8, and after that, the binding energy decreases as lithiation goes on until Li_2S_4, to 0.47 and 0.67 eV. The black dashed curve is the binding energy for c-G computed without vdW functional, which shows the chemical binding strength. It can be seen that for unlithiated S_8, there is almost no chemical interaction, and the adsorption is dominated by vdW physical interaction. For Li_2S_n species, the chemical binding energy is in the range of 0.1–0.3 eV. The E_b evolution profiles suggest that

the chemical interaction mainly comes from the lithium ions, whereas the physical interaction is largely contributed by S atoms. Because the physical interaction in this case is generally stronger than the chemical interaction, the overall adsorption strength gradually decreases with shortening of the lithium polysulfide chain until the Li_2S_2 stage because of relatively large chemical binding. The weakest binding strength appears in the stage of Li_2S_4, before the Li–S compound changes to solid bulk phase, which indicates that the desorption and dissolution of Li_2S_n species has a high probability to take place during lithiation. Although the a-G substrate can induce larger binding strength comparing with crystalline case, the improvement is limited. The E_b value increases by ∼150 meV, and such an improvement can happen only on some special position with certain local environment (see Figure S2 in Supporting Information for detail). The above simulation shows that carbon structure substrate cannot adsorb the Li_2S_n species strongly, especially when the cluster evolve to middle-lithiated stage (around Li_2S_4). Therefore, introducing other materials that can anchor the Li_2S_n species is important.

We calculate the binding strength between Li_2S_n clusters and various layered structure materials. The simulated binding energies E_b with vdW at different lithiation stages are shown as Figure 3a. The particular case of adsorption on TiS_2 material is shown in the "with vdW" side of Figure 3c. For unlithiated S_8 adsorption, these materials can induce the similar binding energy (0.75–0.85 eV) that are also comparable with that on graphene. As soon as the lithiation begin, different materials induce distinct anchoring effect. According to the magnitude of E_b, these materials can be classified into three types: For oxides (V_2O_5 and MoO_3), the binding energies are all very large (>2.0 eV) regardless of the lithiation stage. For sulfides (TiS_2, ZrS_2, VS_2, NbS_2, and MoS_2), the binding strength is not as strong as in the oxides case, but the binding strength is still remarkable. Except for MoS_2, the E_b values for sulfides are all larger than 1.00 eV. For chlorides, the anchoring effect is weak and the E_b values are all smaller than 0.80 eV. Therefore, these three types of materials—namely, oxides, sulfides, and chlorides—can be viewed as strong, moderate, and weak AMs, with the induced binding energies in ranges of 2.0–4.2 eV, 0.8–2.0 eV, and 0.4–0.8 eV, respectively (see Figure S4 in Supporting Information for detailed analysis of AM with different outermost anions). For strong and moderate AMs, the evolutions of E_b follow the similar trend in general. For the strong one, the binding strength grows stronger with increasing lithiation; for the moderate one, the binding strength for Li_2S_6 is smallest among all the Li_2S_n species, but after that, the magnitude of E_b also gradually increases. Both strong and moderate AMs present the opposite to the decreasing trend of carbon-based graphene during lithiation. On the other hand, the anchoring effect of weak AMs is similar to that of graphene (in another word, graphene can be viewed as a weak AM).

It is obvious that the anchoring effect of AM mainly originates from its chemical interaction with the Li atom in Li_2S_n species, which overcomes the weak chemical adsorption by carbon substrate. We estimate the contributions by chemical interaction and physical vdW interaction at difference lithiation stages for five selected AMs. Figure 3b exhibits the ratio for vdW interaction, which is expressed as $R = (E_b^{vdW} - E_b^{no\ vdW})/E_b^{vdW}$ (E_b^{vdW} and $E_b^{no\ vdW}$ represent binding energy computed with and without vdW functional, respectively). For all the AM materials we study, the vdW interaction dominates the unlithiated stage with the ratios of nearly 100%, which means
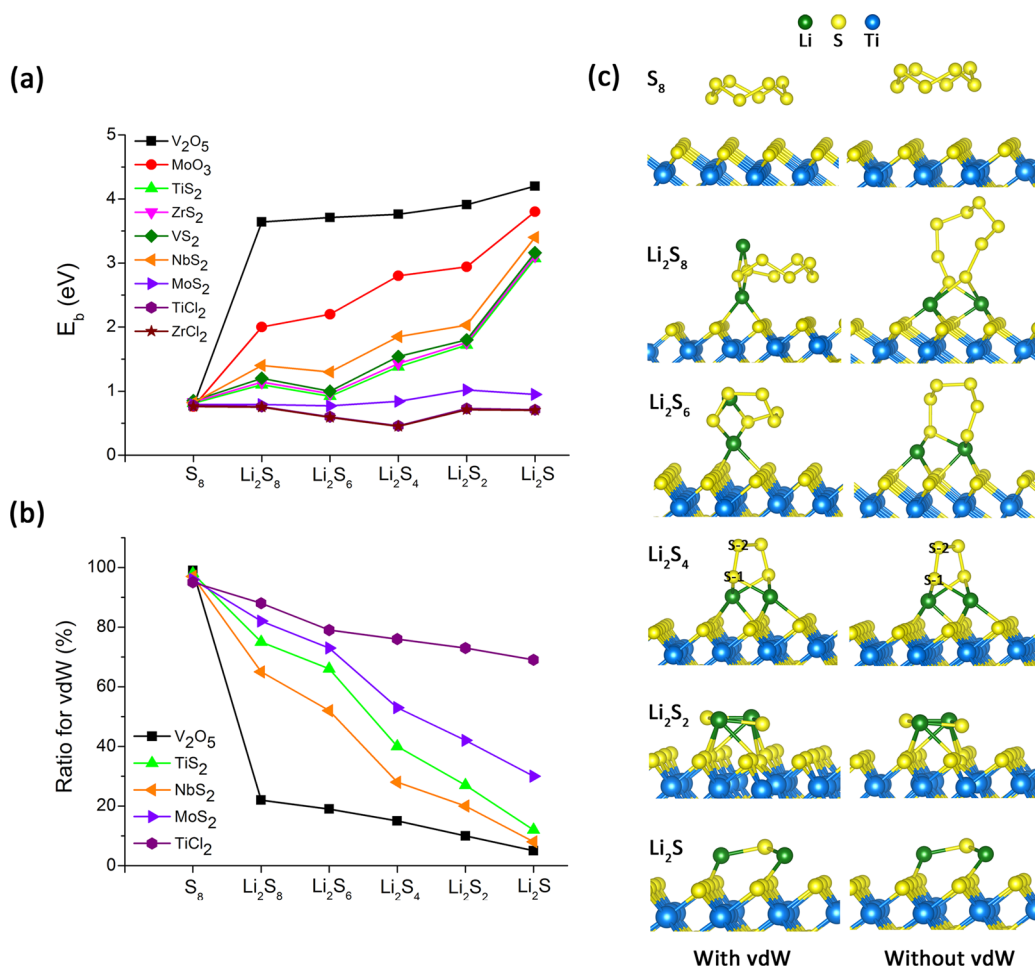
Figure 3. (a) Binding energies for Li−S composites at four different lithation stages (S_8, Li_2S_6, Li_2S_4, Li_2S_2) on different AMs we select. (b) Ratio for vdW interaction for five kinds of extracted AMs at four different lithation stages. (c) Li−S clusters' conformations on TiS_2. Figures on left and right sides are simulated with and without vdW functional.

these AMs cannot form a chemical bond with S atom. Different AMs will lead to distinct conditions as soon as the lithiation begins, although the ratio profiles have the same decreasing trend. For strong AM (V_2O_5), chemical interaction dominates the whole process of lithiation, and the vdW interaction ratio is always lower than 15% and drops slightly to 7% for Li_2S_2. For moderate AMs, physical interaction plays an major role for underlithiated Li_2S_8 and Li_2S_6 stage with the ratio in the region of 52−60%, but after that, physical interaction remains a much smaller percentage from Li_2S_4, in the region of 10−40%. For weak AM ($TiCl_2$), physical interaction dominates the whole process with the ratio larger than 70%, similar to graphene case. The vdW interaction can also influence the adsorption configuration of Li_2S_n species. Figure 3c shows the comparison between the stable configurations for Li_2S_n species on TiS_2 computed with (left side) and without (right side) vdW functional. For the S_8 case, the distance between S_8 cluster and TiS_2 changes from 3.7 to 3.1 Å, due to the inclusion of physical interaction. For Li_2S_8 and Li_2S_6, the adsorption conformation also greatly changes because physical vdW interaction plays the major role, and lying-in-plane configuration, which can enhance physical interaction strength, is favorable. This is also the reason why the binding energy for Li_2S_8 is larger than that of Li_2S_6 because of the longer sulfur chain. For Li_2S_4, Li_2S_2, and Li_2S, the adsorption configurations are almost the same after

introducing vdW interaction because chemical interaction dominates.

The fundamental difference between two kinds of interaction can be visualized from the electron charge transfer analysis. Here, we take the adsorption systems of S_8 and Li_2S_4 on TiS_2 and V_2O_5 for example, and the charge difference after adsorbing is plotted as Figure 4a. For interaction with AM with unlithiated S_8, the charge transfer happens inside the S_8 cluster and inside the AM, but almost no charge exchange exists between them, indicating no formation of chemical bond. In contrast, in the case of Li_2S_4, charge increases between Li atom and O or S atom (pink part), which induces strong chemical bonds (Li−S bond for TiS_2 and Li−O bond for V_2O_5). Meanwhile, charge is lost along the Li−S bond inside Li_2S_4 (green part) and internal Li−S bond softens. Intuitively, the effect of chemical interaction can be also seen from the distortion of Li_2S_4 cluster's configurations (Figure 3c or Figure 4a). For free-standing Li_2S_4 (see Figure 1b), all the sulfur atoms, which can be labeled as the S-1 and S-2 according to the relative position with Li atom, form bonds with Li atom. After introducing strong or moderate AMs, S-2 atoms depart from Li atom and their bonds disappear. Although the S-1 atoms can bind with Li, the S−Li bond lengthens. Table 1 lists the Li−S bond lengths for Li_2S_4 cluster adsorbing on six different AMs. The Li−S bond grows longer as the binding energy grows larger. The distortion of Li_2S_n species indicates that there exists
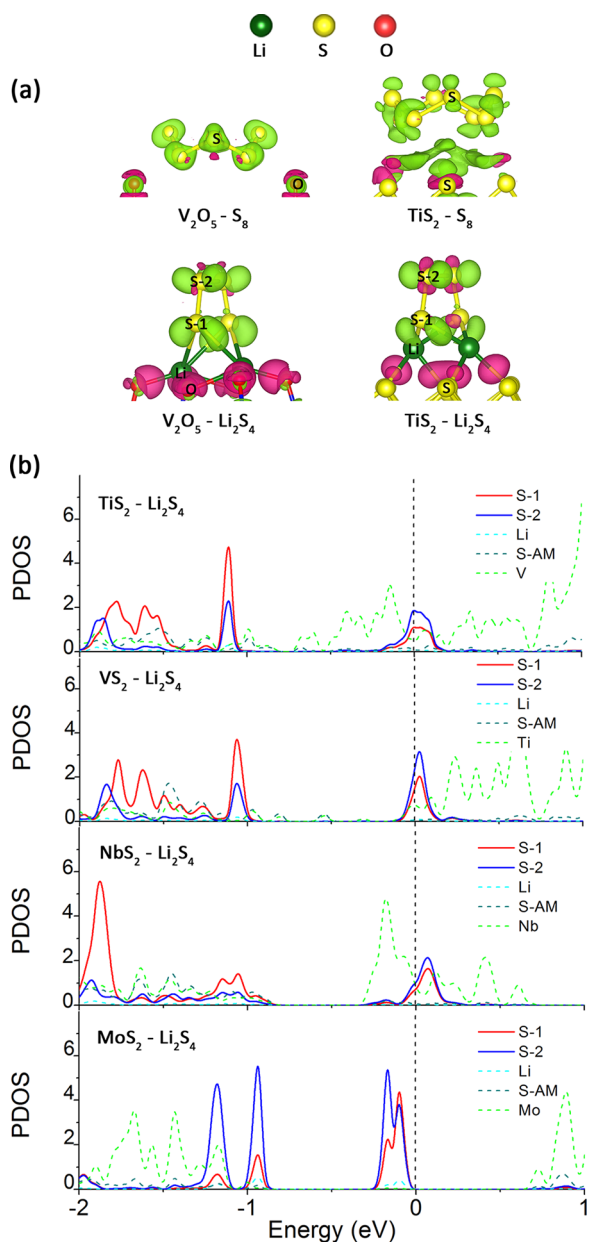
Figure 4. (a) Charge transfers when S_8 or Li_2S_4 adsorbs on V_2O_5 or TiS_2. The charge transfer is the charge difference after and before Li−S cluster is put on AM and can be expressed as $\Delta\rho = \rho(AM + Li_2S_4) - \rho(AM) - \rho(Li_2S_4)$, where $\rho(AM + LiS)$, $\rho(AM)$, and $\rho(Li_2S_4)$ are the charge densities for adsorption system, AM system, and Li−S cluster system, respectively. Here, pink (green) is the spatial regions gain (loss) in charge. (b) Atomic partial density of state near Fermi energy region for Li_2S_4 cluster on disulfides TiS_2, VS_2, NbS_2, and MoS_2.

Table 1. Six Different Layered Materials Are Selected for the Computation of Parameters When Li_2S_4 Cluster Is Adsorbed[a]

	V_2O_5- Li_2S_4	MO_3- Li_2S_4	NbS_2- Li_2S_4	TiS_2- Li_2S_4	MoS_2- Li_2S_4	$TiCl_2-$ Li_2S_4
E_b (eV)	3.73	2.85	1.80	1.54	0.77	0.38
d_{Li-S} (Å)	2.96	2.78	2.65	2.54	2.40	2.38
$\Delta e_{AM} =$ $-\Delta e_{Li-S}$	1.92	1.72	1.25	1.17	0.20	0.05
Δe_{Li}	−0.06	−0.04	−0.01	−0.01	0.00	0.00
Δe_{S-1}	−0.60	−0.51	−0.37	−0.28	−0.10	−0.02
e_{S-1}	6.10	6.24	6.34	6.42	6.66	6.67
e_{S-2}	5.90	5.92	5.92	5.94	6.13	6.16

[a]From top to bottom are binding energies, distances between Li and S-1 atom, Bader charge difference inside AM, Li atom and S-1 atom, and Bader charge magnitudes for S-1 and S-2 atom. Here, Bader charge difference means the difference of charge value between adsorbed case and free-standing case.

Supporting Information for detail). For V_2O_5, the charge transfer amount even approaches to 2.0e, which means all the valence electrons in two Li atoms were attracted to AM. As a result, the Li_2S_4 cluster will be positively charged, whereas the AM will be rich in electrons, and such separation determines the strength of chemical interaction. Furthermore, such charge separation can also induce electrostatic interactions between them, which also enhances the anchoring effect. In Supporting Information Figure S5, we show the Δe_{AM} evolution for each Li_2S_n species ($n = 1-8$) and for different AMs. As lithiation goes on, more and more charge transfers into AM, which is the reason why the chemical binding strength increases as lithiation goes on.

As shown in Table 1, the Δe_{Li} values are very small, whereas Δe_{S-1} values are much larger for nonweak AM, which suggests that the chemical interaction originates from the charge transfer between S atoms in Li_2S_n cluster into the AMs, and as a result, strong Li−AM bond is formed while the Li−S bond inside the cluster is softened. From the charge magnitudes of S-1 and S-2 atoms, it is indicated that as the binding strength grows stronger, the charge difference between S-1 and S-2 becomes smaller, and trends to 6.00e, the valence charge of isolated S atom, in contrast to the free-standing cluster, in which S-1 and S-2 atoms own the charge of 6.71e and 6.17e, respectively. That means Li_2S_n species has the tendency to form Li^+ and S_n^{2-} ions, which readily dissolve into the electrolyte, especially for strong AM like V_2O_5 and MoO_3. Form Figure 4a, it can be seen that the loss of charge near S atoms have the feature of π state, especially for S-2. For free-standing Li_2S_4, an electron in Li atom transfers into S, and the redundant part occupies the π state with high energy, which becomes the highest occupied state. After introducing AM, the electron on this state partially migrates to AM. Figure 4b shows the atomic partial density of state (PDOS) near Fermi energy for the adsorption system of Li_2S_4 on different disulfide materials. Concentrating on the thick red and blue curves, which represent PDOS for S-1 and S-2 atoms, it can be seen that the Fermi energies lie in different location referring to pockets of two atomic states, which means a different amount of charge transfer. The position of Fermi energy agrees with the electron amount variance and determines the binding strengths for these disulfides. For example, for NbS_2, the Fermi energy locates close to left edge of pockets, which causes a large binding energy, but for MoS_2,

competition between Li-AM and Li−S chemical bond, which is associated with electronic structure modification and charge transfer as shown above.

To further investigate the chemical interaction and charge transfer quantitatively, the Bader charge method is applied to achieve the amount of valence electron around the atoms.[46,47] Table 1 lists the variance of charge for atoms in Li_2S_4 cluster or AM after adsorption. The negative value of transfer charge for Li_2S_4 cluster (Δe_{Li-S}) and positive transfer value for AM (Δe_{AM}) shows that the charge migrates from the adsorbed cluster to AM. Detailed analysis shows that the electron is dominantly captured by outmost anions (see Table S1 in

the Fermi energy locates just outside of the right edge and the pockets are almost filled, so the binding is very weak.

The weakening of the Li−S bond and the charge transfer into AM suggests that too strong chemical binding between Li ion and AM is not good news for the performance of Li−S battery, because it can cause decomposition of the Li_2S_n species. Here, we compare the energies between intact and decomposed structures. Two kinds of decomposed structures are studied, they are $Li + LiS_n$ and $Li + Li + S_n$ (Li means isolated Li atom, and $n = 4$ or 6), respectively. V_2O_5, MoO_3, NbS_2, and TiS_2 are extracted from strong AM and moderate AM models for such study, and ΔE_1 and ΔE_2—as listed in Figure 5b and that
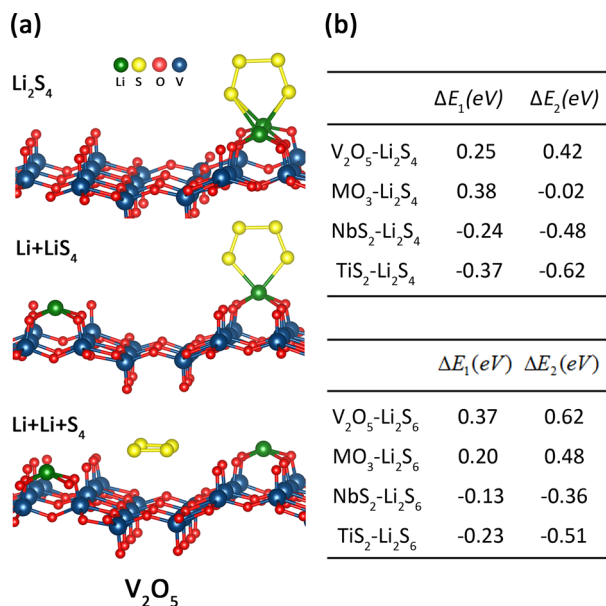

Figure 5. (a) Atomic configurations for Li_2S_4 (up), Li + LiS$_4$ (middle), Li + Li + S$_4$ (down) clusters adsorbed on V_2O_5. (b) Energy differences between intact Li_2S_4 and destructed Li_2S_4's adsorption on V_2O_5. Here, $\Delta E_1 = E(Li_2S_4 + V_2O_5) - E(Li + LiS_4 + V_2O_5)$, and $\Delta E_2 = E(Li_2S_4 + V_2O_5) - E(Li + Li + S_4 + V_2O_5)$, respectively.

	$\Delta E_1 (eV)$	$\Delta E_2 (eV)$
V_2O_5-Li_2S_4	0.25	0.42
MO_3-Li_2S_4	0.38	-0.02
NbS_2-Li_2S_4	-0.24	-0.48
TiS_2-Li_2S_4	-0.37	-0.62

	$\Delta E_1 (eV)$	$\Delta E_2 (eV)$
V_2O_5-Li_2S_6	0.37	0.62
MO_3-Li_2S_6	0.20	0.48
NbS_2-Li_2S_6	-0.13	-0.36
TiS_2-Li_2S_6	-0.23	-0.51

represent the binding energy difference between two kinds of decomposed structures and Li_2S_n—are used to evaluate the stability of intact Li−S cluster. Positive value means that the decomposed configuration owns lower energy than intact one. We extract three kinds of configurations for Li_2S_4's adsorption on V_2O_5 for instance, as shown in Figure 5a. For the Li_2S_4 adsorption case, the decomposed structure is energetically preferable for V_2O_5 and MoO_3 substrates, and ΔE_2 is even larger than ΔE_1 for V_2O_5, which suggests destruction of the Li_2S_4 cluster. For Li_2S_6 adsorption case, the Li + Li + S_6 structures possess the lowest energies for both of them, while intact cluster configuration is the most unstable. For moderate NbS_2 and TiS_2, intact Li_2S_6 cluster conformation can be saved, although the Li−S bond is weaker. According to the comparison between Li_2S_4 and Li_2S_6 cases, the decomposition of Li_2S_n species is easier to happen at underlithiated (Li_2S_6) stage. This is because Li_2S_6 species has weaker chemical interaction with AM, whereas sulfur has stronger physical interaction with AM during this stage.

The decomposition of Li−S cluster means lithium prefer to stay alone instead of forming bond with sulfur and leads to separation of these two elements. Such structure destruction can impair the effect of sulfur, which is the key functional

material in electrode material system. Even worse, the associated weakening of the Li−S bond can induce the thorough separation between lithium and sulfur atom and Li_2S_n species have the tendency to form Li^+ and S_n^{2-} ions, and sulfur material can dissolve into the electrolyte. Therefore, from this point of view, too strong AMs such as V_2O_5 or MoO_3, with the binding strength larger than ∼2.0 eV, might not be good choices. In contrast, moderate AMs can strike a balance between binding strength and intactness of the Li_2S_n species, overcoming the disadvantage of both strong and weak AMs. That is the most likely reason why moderate AMs including TiS_2, ZrS_2, and VS_2 have been demonstrated to induce one of the best cycling performances until now,[36] but many oxide materials, which are predicted to result in stronger binding strength according to the simulations, cannot improve the performance as efficiently as these sulfides in experiments.

From the simulation above, it can be seen that there are still problems remaining after introducing AMs, which possibly explain why the performance of Li−S batteries is still not good enough. First, for unlithiated S_8, the binding strength with AMs is still not strong enough. Second, for underlithiated stage Li_2S_6, the chemical binding with AMs is generally weak except in the case of very strong AMs, but it is easy for such strong AMs to cause deconstruction of Li_2S_n species at this stage. On the basis of the binding energy data and electronic structure properties, some approach to fix them can be tried. For the former problem, using new kinds of AM that enable larger physical adsorption for S_8 is a possible solution. Furthermore, according to the simulation, the amorphous structure of AM can also improve the anchoring effect. For the latter one, using other moderate AMs is a choice. NbS_2 may be better comparing with TiS_2, VS_2, and ZrS_2 in the aspect of larger binding energy, especially for Li_2S_8 and Li_2S_6 stages (see Figure 3a). Beyond the optimization of AM, we can also take advantage of the charge separation in Li_2S_n−AM material system. Because Li_2S_n species and AM are positively and negatively charged, there must be strong dipole inside, and for stabilizing Li_2S_n−AM material system, the polar substrate can be very useful.

■ CONCLUSION

In conclusion, we have applied the entire-lithiation-process computation and presented a detailed study on the anchoring effect of various layered-structured materials. Different materials lead to distinct adsorption features with Li_2S_n species, whereas the binding strength is determined by the amount of charge transfer from S atoms in cluster into the AM. The anchoring is always accompanied by the softening of Li−S bonds, and too strong binding can induce the destruction of Li_2S_n species. Our work explores the reason why carbon substrate, like graphene, cannot firmly adhere Li_2S_n species and reveals the mechanism for anchoring effect for different lithiated Li_2S_n species at the atomic level. On the basis of the computation, we suggest moderate AMs are the best choices for battery electrode. These materials can induce remarkable but not too strong binding strength (physical-dominated interaction for underlithiation stage and chemical-dominated interaction after that), and particularly, save the intact Li_2S_n configuration and avoid its dissolution into the electrolyte. Furthermore, we give advice theoretically on the way to settle the unsolved issues, which could be meaningful for the further improvement of the battery performance.

■ ASSOCIATED CONTENT

Ⓢ Supporting Information

Methods and Descriptions of simulation results. The Supporting Information is available free of charge on the ACS Publications website at DOI: 10.1021/acs.nanolett.5b00367.

■ AUTHOR INFORMATION

Corresponding Authors

*E-mail: qianfan@buaa.edu.cn.

*E-mail:yicui@stanford.edu.

Notes

The authors declare no competing financial interest.

■ ACKNOWLEDGMENTS

■ REFERENCES

(1) Whittingham, M. S. *Chem. Rev.* **2004**, *104*, 4271−4301.

(2) Kang, B.; Ceder, G. *Nature* **2009**, *458*, 190−193.

(3) Chiang, Y. M. *Science* **2010**, *330*, 1485−1486.

(4) Zhao, K.; Wang, W. L.; Gregoire, J.; Pharr, M.; Suo, Z.; Vlassak, J. J.; Kaxiras, E. *Nano Lett.* **2011**, *11*, 2962−2967.

(5) Goodenough, J. B.; Park, K. S. *J. Am. Chem. Soc.* **2013**, *135*, 1167−1176.

(6) Yin, Y.-X.; Xin, S.; Guo, Y.-G.; Wan, L.-J. *Angew. Chem., Int. Ed.* **2013**, *52*, 13186−13200.

(7) Bruce, P. G.; Freunberger, S. A.; Hardwick, L. J.; Tarascon, J. M. *Nat. Mater.* **2012**, *11*, 19−29.

(8) Yang, Y.; Zheng, G.; Cui, Y. *Chem. Soc. Rev.* **2013**, *42*, 3018−3032.

(9) Mikhaylik, Y. V.; Akridge, J. R. *J. Electrochem. Soc.* **2004**, *151*, A1969−A1976.

(10) Ji, X. L.; Nazar, L. F. *J. Mater. Chem.* **2010**, *20*, 9821−9826.

(11) Barchasz, C.; Lepretre, J. C.; Alloin, F.; Patoux, S. *J. Power Sources* **2012**, *199*, 322−330.

(12) Shim, J.; Striebel, K. A.; Cairns, E. J. *J. Electrochem. Soc.* **2002**, *149*, A1321−A1325.

(13) Jung, D. S.; Hwang, T. H.; Lee, J. H.; Koo, H. Y.; Shakoor, R. A.; Kahraman, R.; Jo, Y. N.; Park, M.-S.; Choi, J. W. *Nano Lett.* **2014**, *14*, 4418.

(14) Seh, Z. W.; Wang, H.; Liu, N.; Zheng, G.; Li, W.; Yao, H.; Cui, Y. *Chem. Sci.* **2014**, *5*, 1396.

(15) Yao, H.; Yan, K.; Li, W.; Zheng, G.; Kong, D.; She, Z. W.; Narasimhan, V. K.; Liang, Z.; Cui, Y. *Energy Environ. Sci.* **2014**, *7*, 3381.

(16) Sun, Y.; Seh, Z. W.; Li, W.; Yao, H.; Zheng, G.; Cui, Y. *Nano Energy* **2015**, *11*, 579.

(17) Xin, S.; Gu, L.; Zhao, N.-H.; Yin, Y.-X.; Zhou, L.-J.; Guo, Y.-G.; Wan, L.-J. *J. Am. Chem. Soc.* **2012**, *134*, 18510.

(18) Qiu, Y.; Li, W.; Zhao, W.; Li, G.; Hou, Y.; Liu, M.; Zhou, L.; Ye, F.; Li, H.; Wei, Z.; Yang, S.; Duan, W.; Ye, Y.; Guo, J.; Zhang, Y. *Nano Lett.* **2014**, *14*, 4821.

(19) Ji, X.; Lee, K. T.; Nazar, L. F. *Nat. Mater.* **2009**, *8*, 500−506.

(20) Jayaprakash, N.; Shen, J.; Moganty, S. S.; Corona, A.; Archer, L. A. *Angew. Chem., Int. Ed.* **2011**, *50*, 5904−5908.

(21) Schuster, J.; He, G.; Mandlmeier, B.; Yim, T.; Lee, K. T.; Bein, T.; Nazar, L. F. *Angew. Chem., Int. Ed.* **2012**, *51*, 3591−3595.

(22) Zheng, G.; Yang, Y.; Cha, J. J.; Hong, S. S.; Cui, Y. *Nano Lett.* **2011**, *11*, 4462−4467.

(23) Guo, J.; Xu, Y.; Wang, C. *Nano Lett.* **2011**, *11*, 4288−4294.

(24) Elazari, R.; Salitra, G.; Garsuch, A.; Panchenko, A.; Aurbach, D. *Adv. Mater.* **2011**, *23*, 5641−5644.

(25) Su, Y. S.; Manthiram, A. *Nat. Commun.* **2012**, *3*, 1166.

(26) Zheng, G.; Zhang, Q.; Cha, J. J.; Yang, Y.; Li, W.; Seh, Z. W.; Cui, Y. *Nano Lett.* **2013**, *13*, 1265−1270.

(27) Seh, Z. W.; Zhang, Q. F.; Li, W. Y.; Zheng, G. Y.; Yao, H. B.; Cui, Y. *Chem. Sci.* **2013**, *4*, 3673−3677.

(28) Li, W. Y.; Zhang, Q. F.; Zheng, G. Y.; Seh, Z. W.; Yao, H.; Cui, Y. *Nano Lett.* **2013**, *13*, 5534−5540.

(29) Ji, L.; Rao, M.; Zheng, H.; Zhang, L.; Li, Y.; Duan, W.; Guo, J.; Cairns, E. J.; Zhang, Y. *J. Am. Chem. Soc.* **2011**, *133*, 18522−18525.

(30) Song, M. S.; Han, S. C.; Kim, H. S.; Kim, J. H.; Kim, K. T.; Kang, Y. M.; Ahn, H. J.; Dou, S. X.; Lee, J. Y. *J. Electrochem. Soc.* **2004**, *151*, A791−A795.

(31) Choi, Y. J.; Jung, B. S.; Lee, D. J.; Jeong, J. H.; Kim, K. W.; Ahn, H. J.; Cho, K. K.; Gu, H. B. *Phys. Scr.* **2007**, *T129*, 62−65.

(32) Kim, J.-S.; Hwang, H. T.; Kim, B. G.; Min, J.; Choi, J. W. *Adv. Funct. Mater.* **2014**, *24*, 5359−5367.

(33) Demir-Cakan, R.; Morcrette, M.; Nouar, F.; Davoisne, C.; Devic, T.; Gonbeau, D.; Dominko, R.; Serre, C.; Feryey, G.; Tarascon, J. M. *J. Am. Chem. Soc.* **2011**, *133*, 16154−16160.

(34) Seh, Z. W.; Li, W.; Cha, J. J.; Zheng, G.; Yang, Y.; McDowell, M. T.; Hsu, P. C.; Cui, Y. *Nat. Commun.* **2013**, *4*, 1331.

(35) X, Han; Y, Xu; Chen, X.; Chen, Y.-C.; Weadock, N.; Wan, J.; Zhu, H.; Liu, Y.; Li, H.; Rubloff, G.; Wang, C.; Hu, L. *Nano Energy* **2013**, *2*, 1197.

(36) Seh, Z. W.; Yu, J. H.; Li, W.; Hsu, P.; Wang, H.; Sun, Y.; Yao, H.; Zhang, Q.; Cui, Y. *Nat. Commun.* **2014**, *5*, 5017.

(37) Kresse, G.; Hafner, J. *Phys. Rev. B* **1993**, *48*, 13115−13118.

(38) Kresse, G.; Furthmuller, J. *Phys. Rev. B* **1996**, *54*, 11169−11186.

(39) Blochl, P. E. *Phys. Rev. B* **1994**, *50*, 17953−17979.

(40) Perdew, J. P.; Burke, K.; Ernzerhof, M. *Phys. Rev. Lett.* **1996**, *77*, 3865−3868.

(41) Klimes, J.; Bowler, D. R.; Michaelides, A. *J. Phys.: Cond. Matt.* **2010**, *22*, 022201.

(42) Lee, K.; Murray, E. D.; Kong, L.; Lundqvist, B. I.; Langreth, D. C. *Phys. Rev. B* **2010**, *82*, 081101.

(43) *Progress in Intercalation Research*; Müller-Warmuth, W.; Schöllhorn, R., Eds.; Kluwer Academic Publishers: The Netherlands, 1994.

(44) Barchasz, C.; Molton, F.; Duboc, C.; Lepretre, J.; Patoux, S.; Alloin, F. *Anal. Chem.* **2012**, *84*, 3973−3980.

(45) Wang, L.; Zhang, T.; Yang, S.; Cheng, F.; Liang, J.; Chen, J. *J. Energy. Chem.* **2013**, *22*, 72−77.

(46) Henkelman, G.; Arnaldsson, A.; Jonsson, H. *Comput. Mater. Sci.* **2006**, *36*, 254−360.

(47) Tang, W.; Sanville, E.; Henkelman, G. *J. Phys.: Condens. Matter* **2009**, *21*, 084204.